Journal of Instrumentation

A multichannel neutron flux monitoring system for a boron neutron capture therapy facility

Published by IOP Publishing for Sissa Medialab

Received: *October 11, 2019*
Accepted: *November 16, 2019*
Published: *December 5, 2019*

A multichannel neutron flux monitoring system for a boron neutron capture therapy facility

T.A. Bykov,[a,b] **D.A. Kasatov,**[a,b] **A.M. Koshkarev,**[a,b] **A.N. Makarov,**[a,b] **V.V. Porosev,**[a,b,1] **G.A. Savinov,**[a] **I.M. Shchudlo**[a,b] **and S.Y. Taskaev**[a,b]

[a] *Budker Institute of Nuclear Physics, Lavrentiev ave. 11, Novosibirsk 630090, Russia*
[b] *Novosibirsk State University, Pirogova st. 2, Novosibirsk 630090, Russia*

E-mail: porosev@inp.nsk.su

Abstract: The progress in the design of new accelerator-based neutron sources for boron neutron capture therapy (BNCT) generated new requirements to the detector systems to monitor the particle flux during the irradiation of patients. In the current research, we evaluated basic parameters of a twin scintillator-over-fiber system with a silicon photo-multiplier readout based on boron-enriched and boron-free plastic scintillators. The presented results showed that the proposed system could be used for monitoring of neutron flux, and the designed detector system demonstrated good linearity, up to ~ 2 mA, limited by accelerator specifications at that time.

Keywords: Detector modelling and simulations I (interaction of radiation with matter, interaction of photons with matter, interaction of hadrons with matter, etc); Instrumentation for hadron therapy; Neutron detectors (cold, thermal, fast neutrons); Scintillators, scintillation and light emission processes (solid, gas and liquid scintillators)

[1] Corresponding author.

https://doi.org/10.1088/1748-0221/14/12/P12002

2019 JINST 14 P12002

Contents

2019 JINST 14 P12002

1 Introduction

The advent of a new generation of the accelerator-based epithermal neutron sources for BNCT raised the question of new diagnostic methods to control the contribution of neutrons to the total radiation dose of patients. The most common approach to solving this problem is using two detectors simultaneously: the first one, sensitive to gamma radiation, and the second one, sensitive to gamma radiation and neutrons. The difference in readings of these two detectors allows us to estimate the contribution of the neutron component more accurately [1]. Plastic scintillation detectors with an optical fiber readout are successfully used for gamma and high-energy electron dosimetry [2]. A similar approach for neutrons was developed in Japan [3, 4]. In this research, we tested the basic parameters of a scintillator-over-fiber detector with a silicon photomultiplier (SiPM) readout. The application of the SiPMs instead of vacuum photo-multipliers has several advantages. First, they are more compact, have excellent single photo-electron resolution and higher quantum efficiency, and are chipper by far. Additionally, progress in the design of a related readout electronics made it possible to create multichannel readout systems based on dedicated ASICs. Further, we present our results on the creation of a dose monitoring system for a proton tandem accelerator with a lithium neutron producing target, proposed at BINP [5].

2 Scintillators and optical fibers

Two types of polystyrene-based scintillators: SC-301, without boron, and SC-331, enriched with boron, which have a fast response of ~ 2.5 ns, are produced in Russia [6]. According to their specifications, both of them use the same fluorophores and SC-331 contains 0.9% natural isotope Boron-10. The maximum of the emission spectrum of the scintillator is situated near 425 nm. The light yield of SC-331 is 8600 photons/MeV, and for SC-301 it is approximately 25 % higher.

Polymer-based Optical Fibers (POFs) are widely used for data communications. One of the most popular materials used for their production is polymethylmethacrylate (PMMA). Polystyrene (PS) or polycarbonate-based fibers have a higher refraction index, but because of higher attenuation they are not generally used for data communications. Main parameters of the tested POFs with a diameter of 1 mm are presented in the table 1.

Table 1. Main parameters of the tested POFs.

Name	Numerical aperture	Core material
ASAHI, SB-1000	0.60	PMMA
MITSUBISHI, CK-40	0.50	PMMA
KURARAY, CLEAR-PSMSJ	0.72	PS

Figure 1 demonstrates the light transmission as a function of the POF length, measured at a wavelength of 405 nm. The solid lines in the figure show the calculated fraction of transmitted light depending on the fiber length with a characteristic absorption length of 1.8 meter (curve 1) and 26.5 meter (curve 2). The measurements were done on a stand with a LED driver SP5601 (CAEN)[1] as a light source. Transmitted optical pulses were detected by MPPC S13360-3050CS (HAMAMATSU), followed by a home-made amplifier based on THS3202 (Texas Instruments)[2] with a gain of ~ 20. Amplified signals were recorded with a desktop waveform digitizer DT5720 (CAEN). All PMMA-based fibers exhibit similar behavior with transmission of ~ 70% signal at a distance of ~ 9 m, while the polystyrene-based fiber showed more significant signal degradation.

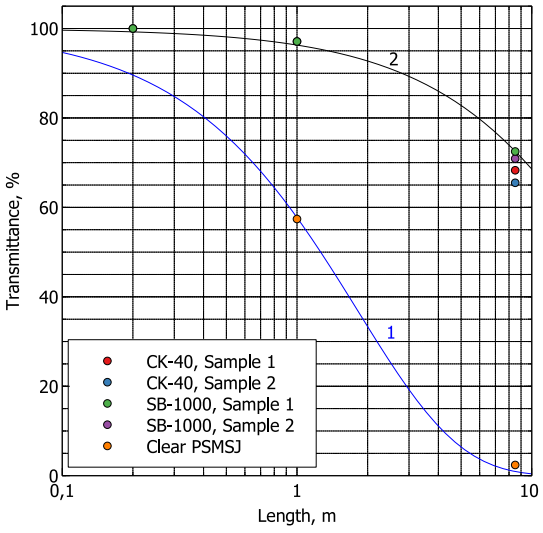

Figure 1. Light transmission of POFs under study.

[1] https://www.caen.it.
[2] http://www.ti.com.

2019 JINST 14 P12002

3 Sensor set-up

To estimate the fraction of optical photons detected at the distal end of a POF when the scintillator is irradiated by thermal neutrons, we performed Monte-Carlo simulations with Geant4-10.5 for two detector geometries, which are shown in figure 2.

Figure 2. Tested scintillator geometries.

Because we planned to use small scintillator samples ~ 1 mm^3, we decided to revise data on their emission spectra. The main reason is the fact that the excitation energy of the primary fluorophore is transferred to molecules of the spectrum shifter by the radiation transfer. For small scintillator samples of ~ 150 µm, the probability of these UV photons escaping from the sensitive detector volume can no longer be considered negligible [7]. Unfortunately, the detection efficiency of plastic scintillators is significantly smaller in comparison with inorganic single crystals and thus it is rather hard to get reliable data under X-rays for small samples. Therefore, we just tested samples with dimensions of $9 \times 9 \times 5$ mm and $9 \times 9 \times 1$ mm. All the faces of the scintillators were mechanically polished. The top and side faces were coated with the EJ-510 paint. The measurements of the emission spectra of scintillator under X-rays were carried out on a stand based on the monochromator MDR-12U (LOMO, St.Petersburg), equipped with a photon-counting head H9319-01 (HAMAMATSU). The scintillators were irradiated by an X-ray tube at 100 kVp. Additionally, we compared the emission spectra when the scintillator was excited by an ultraviolet (UV) light-emitting diode (UVTOP300-HL-TO39, ROITHNER LASERTECHNIK GmbH)[3] with a wavelength of 305 nm, near the maximum of photoabsorption of the primary fluorophore. In this case, the fluorescence spectra of the scintillator were measured by two methods: light transmission through a sample and light reflectance from a sample. Figure 3 demonstrates the emission spectra of the scintillator under different conditions.

It is seen that under X-rays a thinner sample demonstrates a noticeable light output at a wavelength of less than 420 nm. The behavior of the emission spectra under UV excitation depends strongly on the layout. In the transmission method, we can observe significant self-absorption at lower wavelengths. In the reflection method, we can see significant contribution from the primary fluorophore of the scintillator with a maximum near 360 nm. In our later research, we used an X-ray excited emission spectrum for a 1 mm sample.

In the simulations, we compared two types of scintillator surfaces: the ground-back-painted to describe the diffuse light scattering of the white paint EJ-510 (Eljen Technology)[4] and polished aluminum.

[3] http://www.roithner-laser.com.
[4] https://eljentechnology.com.

2019 JINST 14 P12002

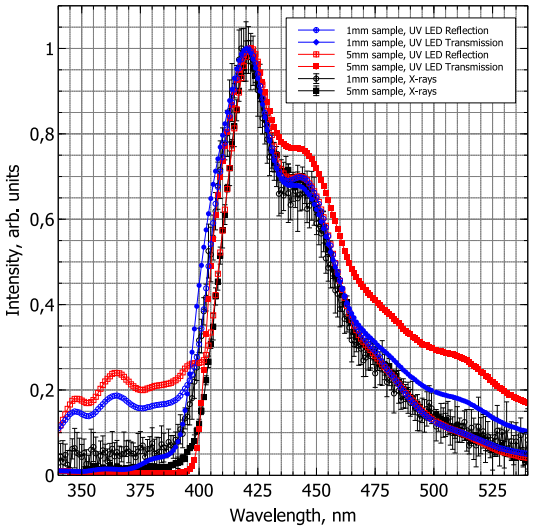

Figure 3. Light emission spectra of SC-301 scintillator under different conditions.

We used the following settings for the stepping process for all particles (e+-, muons/hardons) in the scintillator: the maximum fraction of energy loss in a step of 0.1, a maximum step of 5 μm, a 'Production Cut' parameter of 5 μm, and a Birks constant of 0.133 mm/MeV. This combination of parameters provided realistic results in comparison with experimental data that were obtained during evaluations of scintillator materials [8].

The POF was simulated as a PMMA core with a diameter of 980 μm, cladding 10 μm thick made of amorphous fluoropolymer CYTOP,[5] and outer coating made of black polyethylene. The length of POFs was 8.5 m. Spectral data on PMMA absorption length were reconstructed from technical data on PMMA-based ESKA polymer optical fiber (MITSUBISHI CHEMICAL). To extend the CYTOP refraction data to the visible wavelength range, the manufacturer data were approximated by the following equation:

$$n^2 - 1 = \frac{2.63483 \cdot \lambda^2}{3.09517 \cdot \lambda^2 - 0.0028} - \frac{0.17975 \cdot \lambda^2}{1.97329 \cdot \lambda^2 + 0.33579}, \tag{3.1}$$

where λ is expressed in μm. In the simulations, the optical contact between the scintillator and POF was filled with the most popular technical polymeric material, polydimethylsiloxane with a thickness of 10 μm. The main properties of the optical components with references are presented in table 2.

As a photosensor, we planned to use a MPPC S13360-3050CS. Therefore its quantum efficiency was taken from manufacturer data [17] and was used to describe the sensitivity of a light detector installed at the distal end of the POF. The results of the simulation and the expected numbers of detected optical photons are shown in table 3.

The low probability of light capture by the optical fiber leads to the fact that only ~ 5 percent of optical photons produced in the scintillator will be detected. The application of aluminum coating on the scintillator ensures no benefits over the white paint. Although a semi-ball shaped scintillator

[5] http://www.agc-chemicals.com/jp/en/fluorine/products/detail/index.html?pCode=JP-EN-F019.

2019 JINST 14 P12002

Table 2. Main parameters of optical materials used in the simulations.

Parameter	Value	Source
EJ-510 Reflection	depending on wavelength	[9]
EJ-510 Refraction index	1.61	[10]
Polystyrene refraction index	depending on wavelength	[11]
Polystyrene absorption length	depending on wavelength	[12]
Polydimethylsiloxane refraction index	depending on wavelength	[13]
PMMA Refraction index	depending on wavelength	[14]
PMMA absorption length	depending on wavelength	[15]
CYTOP Refraction index	depending on wavelength	[16]
CYTOP absorption length	100 m	

Table 3. Expected number of detected optical photons in different configurations. For comparison, when a neutron is captured by a boron atom in the scintillator, ~ 630 photons are produced.

Shape	Coating	Number of detected optical photons
Cylinder, POF length of 8.5 m	All sides: EJ-510	33.7
Cylinder	Side walls: EJ-510, Top: Al reflector	28.9
Cylinder	Side walls: Al reflector, Top: EJ-510	25.6
Cylinder	All sides: Al reflector	15.6
Semi-ball	EJ-510	35.3
Semi-ball	Al reflector	19.4

suggests a slightly higher signal value, in further experiments, we used cylindrical scintillators, which are easier in production.

4 Initial trials

To evaluate this detector approach we made several tests at the BINP BNCT facility. The cylindrical scintillators with a diameter of 1 mm and a length of 1 mm were cut from scintillator blocks. The output window of the scintillator was polished and the other sides were coated with the EJ-510 paint. The scintillators were assembled with POFs with the length of 8.5 m and protected from ambient light by a light-tight housing. The optical coupling between a scintillator and POF was the optical grease BC-630 (Saint-Gobain Crystals).[6] The detectors were installed at a distance of ~ 20 cm from the neutron producing target. Optical pulses were detected by MPPC S13360-3050CS (HAMAMATSU), followed by a home-made amplifier based on THS3202 (Texas Instruments), and processed by a digital acquisition system DT5790 (CAEN) in the charge-integration mode with a gate of 32 ns. During the tests, the temperature of the MPPC was stabilized at 0° C.

[6] https://www.crystals.saint-gobain.com/products/assembly-materials.

2019 JINST 14 P12002

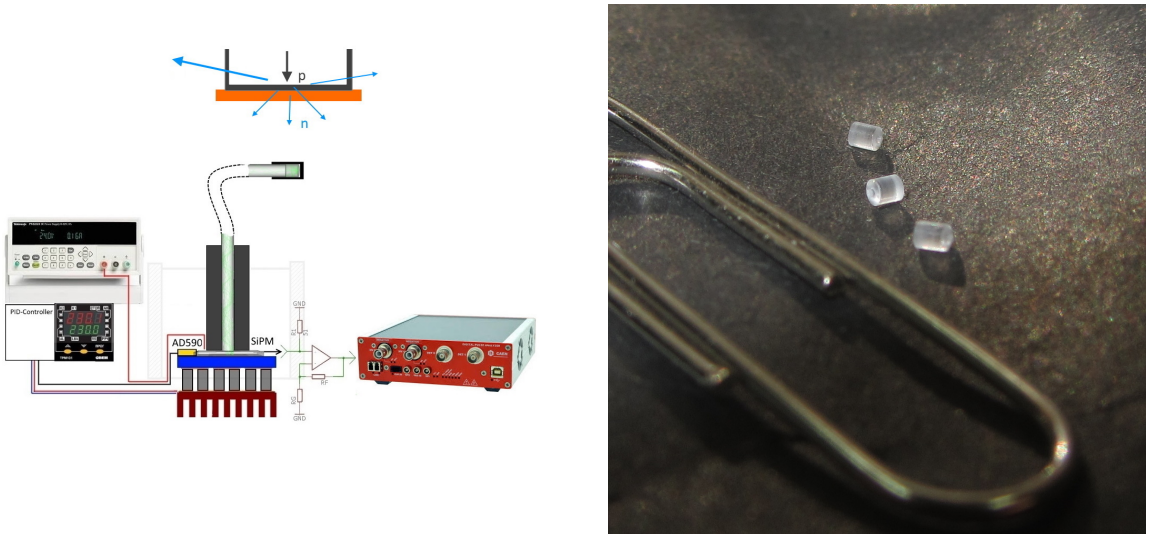

Figure 4. Experimental setup and produced scintillator samples just after mechanical processing.

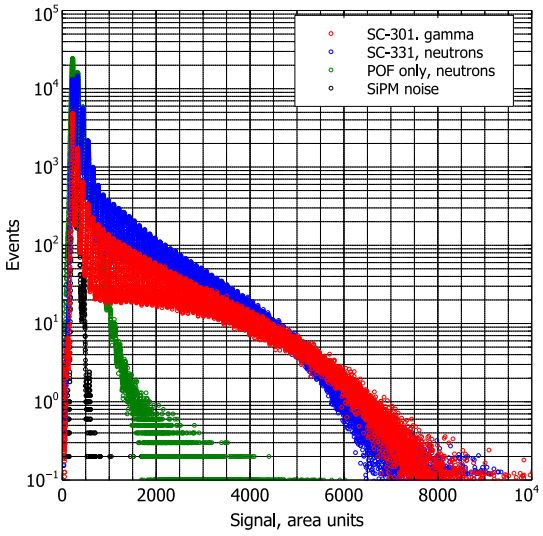

Figure 5. Measured charge spectra in different irradiation conditions.

Figure 4 demonstrates the experimental setup (left) and produced scintillator samples just after cutting (right).

Figure 5 shows examples of the measured spectra: the SiPM noise when the accelerator was off; signals from the SC-301 scintillators when the accelerator operated below the neutron production threshold; signals from the SC-331 (boron-enriched) scintillators when the accelerator operated in the neutron production mode; signals from a POF without scintillator under neutron irradiation, the surface that opposite to its exit window coated with the white paint. From the presented data we can see that in the region of signals below ~ 10 photo-electrons, the intrinsic SiPM noise and the Cherenkov light generated by the secondary high-energy electrons in the optical fiber give a dominant contribution. When the accelerator operates in the neutron production mode,

2019 JINST 14 P12002

the spectrum from the SC-331 scintillator demonstrates an excess of low amplitude events, but the detected neutrons do not form a clearly distinguished peak against the background.

5 Dual threshold approach

The fact that boron-enriched and boron-less scintillators have slightly different light outputs leads to necessity of different detection thresholds in the readout electronics. A neutron-gamma counting detector was realized based on EASIROC ASIC [18]. The EASIROC channel integrates an 8-bit DAC, a variable gain preamplifier, and a fast shaper (15 ns), followed by a discriminator. In our design, two ASICs were connected in parallel to have the possibility of counting the same events with two different thresholds. Four MPPC S13360-3050CS and two pairs of scintillator-over-fiber detectors formed two neutron detection channels. In one pair we used the ASAHI SB-1000 optical fiber and in the second one MITSUBISHI CK-40. The data were continuously accumulated in a 5 ms interval and sent to the computer for further processing. During the operation, the control software measured the environmental temperature and adjusted the bias voltage to keep the SiPM gain constant. Figure 6 demonstrates a simplified block diagram of the detector electronics (left) and the experimental setup (right).

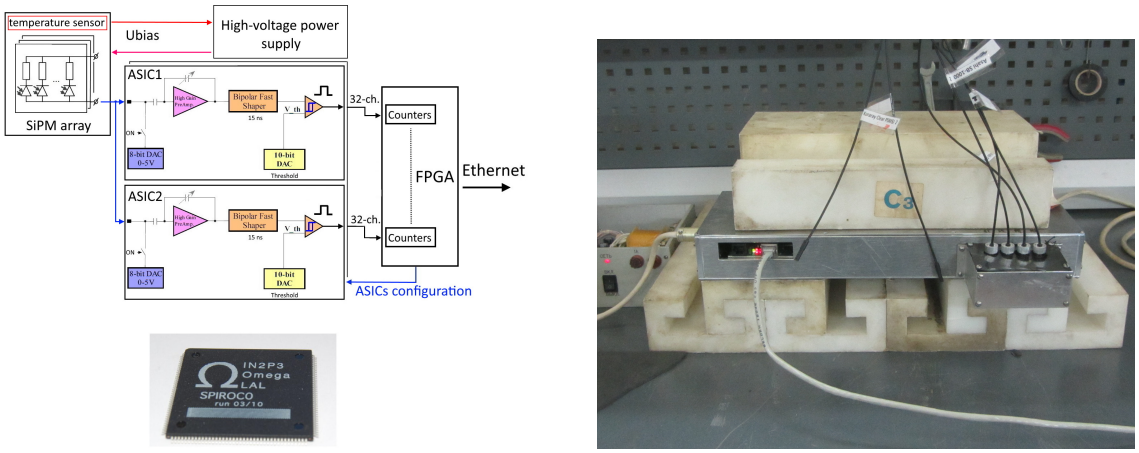

Figure 6. Simplified block diagram of multichannel system and experimental setup.

6 Results and discussion

Figure 7 demonstrates the average count rate per 5 ms as a function of the threshold when the accelerator operates in the neutron production mode.

When the threshold value is less than ~ 200 DAC units, the contribution of the neutron component is visible in the data from registration channels using a scintillator with boron. For regular operation, we adjusted the detection threshold of ASICs near ~ 50 DAC units so that when both detectors (with and without boron) were irradiated with gamma radiation only, they recorded the same event rates. The true value of the neutron flux was restored as the difference between

2019 JINST 14 P12002

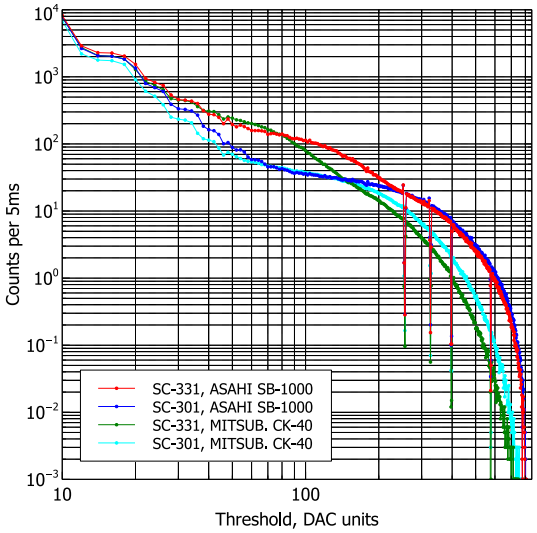

Figure 7. Mean signal value in detector channels per 5 ms vs. detection threshold under neutron irradiation.

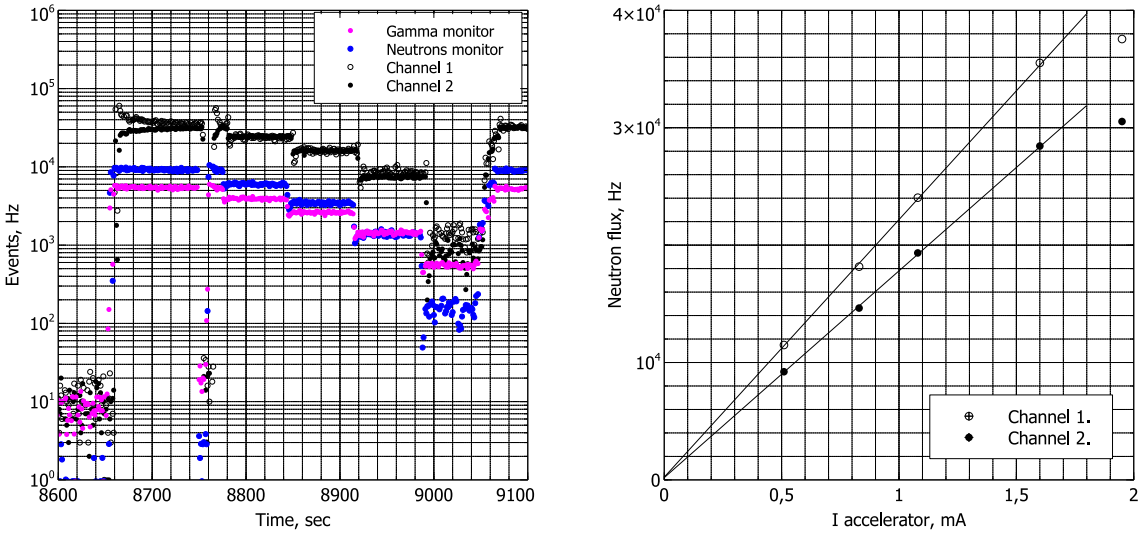

Figure 8. Sample of real-time measurements of neutron flux on BNCT facility (left) and detected neutron flux in detector channels as a function of accelerator current (right).

the counting rates in the ASIC1 channels registering the signal from the scintillator enriched with boron and the counting rates in the corresponding ASIC2 channels recording the signal from the conventional scintillator.

Figure 8(left) shows a sample of the real-time measurements of the thermal neutron flux when the accelerating voltage of the BNCT facility was gradually decreased below the neutron production threshold. For comparison, data from an independent gamma-neutron detection system based on a cerium-activated lithium-silicate glass scintillator with a photomultiplier readout are added [19]. Figure 8(right) demonstrates the signal dependence on the accelerator current for a stationary proton beam with an energy of 2 MeV. The detector demonstrated a good linearity of up to $\sim$ 1.7 mA,

2019 JINST 14 P12002

which was limited by the technical specifications of the accelerator at that time. It is planned that future modifications of the accelerator will operate at up to 10 mA and the detector linearity should be revised. From the last figure it is seen that the two detectors have different responses. The explanation is the fact that the detectors have slightly different sensitivities. Another reason is the difference in the magnitude of the neutron flux at the locations of the detectors, which can vary when the proton beam is positioned on the target. Another important pending issue is the efficiency of light collection on a photodetector. The magnitudes of signals observed in the experiment from neutrons captured in the scintillator were about 2 times less than expected from the simulation. The main reason can be in the production technology of such small scintillator samples. This time we mechanically cut the samples from rather big blocks and polished the output window to provide optical transparency only. In the future, this production stage should be revised to provide well reproducible results.

7 Conclusion

In this study, we tested the scintillator-over-fiber approach to design a neutron sensitive detector for the BNCT. The presented results showed that the proposed system could be used successfully for the monitoring of neutron flux. The application of SiPM instead of vacuum photomultipliers dramatically simplified the detector design and made it possible to realize a compact multichannel readout system. Anyway, there are several issues to address to ensure reliable operation of the detector. In particular, it is necessary to optimize the design of the detector to ensure maximum signal magnitude and to study the long-term stability of the detector components.

Acknowledgments

We would like to thank the BINP BNCT team for their help during the test sessions. The research is partially supported by a grant of the Russian Science Foundation (project №19-72-30005).

References

[1] D. Moro et al., *BNCT dosimetry performed with a mini twin tissue-equivalent proportional counters (TEPC)*, *Appl. Radiat. Isot.* **67** (2009) 171.

[2] A.S. Beddar, T.R. Mackie and F.H. Attix, *Water-equivalent plastic scintillation detectors for high-energy beam dosimetry: I. Physical characteristics and theoretical considerations*, *Phys. Med. Biol.* **37** (1992) 1883.

[3] M. Ishikawa et al., *Early clinical experience utilizing scintillator with optical fiber (SOF) detector in clinical boron neutron capture therapy: Its issues and solutions*, *Radiat. Oncol.* **11** (2016) 105.

[4] M. Ishikawa et al., *Development of real-time thermal neutron monitor using boron-loaded plastic scintillator with optical fiber for boron neutron capture therapy*, *Appl. Radiat. Isot.* **61** (2004) 775.

[5] D. Kasatov et al., *The accelerator neutron source for boron neutron capture therapy*, *J. Phys. Conf. Ser.* **769** (2016) 012064.

[6] V. Rykalin et al., *Development of the Polystyrene Scintillator Technology and Particle Detectors on Their Base*, *J. Phys. Sci. Appl.* **5** (2015) 6.

2019 JINST 14 P12002

[7] R.N. Nurmukhametov et al., *Fluorescence and absorption of a polystyrene-based scintillator exposed to UV laser radiation*, *J. Appl. Spectrosc.* **74** (2007) 824.

[8] V.V. Porosev and G.A. Savinov, *Evaluation of boron-enriched plastic scintillator for thermal neutron detection*, 2019 *JINST* **14** P06003.

[9] Eljen Technology, https://eljentechnology.com/products/accessories/ej-510-ej-520.

[10] M. Janecek and W.W. Moses, *Simulating Scintillator Light Collection Using Measured Optical Reflectance*, *IEEE Trans. Nucl. Sci.* **57** (2010) 964.

[11] https://refractiveindex.info/?shelf=3d&book=plastics&page=ps.

[12] J. Argyriades et al., *Spectral modeling of scintillator for the NEMO-3 and SuperNEMO detectors*, *Nucl. Instrum. Meth.* **A 625** (2011) 20 [arXiv:1004.3779].

[13] https://refractiveindex.info/?shelf=organic&book=polydimethylsiloxane&page=Schneider-Sylgard184.

[14] https://refractiveindex.info/?shelf=organic&book=poly(methyl_methacrylate)&page=Szczurowski.

[15] Mitsubishi Chemical Corporation, https://www.pofeska.com/pofeskae/download/pdf/technical%20data_01.pdf.

[16] Asahi Glass Company, http://www.agc-chemicals.com/file.jsp?id=jp/en/fluorine/products/cytop/download/pdf/CYTOP_EN_Brochure.pdf.

[17] https://www.hamamatsu.com/resources/pdf/ssd/s13360_series_kapd1052e.pdf.

[18] S. Callier, C.D. Taille, G. Martin-Chassard and L. Raux, *EASIROC, an Easy & Versatile ReadOut Device for SiPM*, *Phys. Procedia* **37** (2012) 1569.

[19] V. Aleynik et al., *New technical solution for using the time-of-flight technique to measure neutron spectra*, *Appl. Radiat. Isot.* **69** (2011) 1639.

2019 JINST 14 P12002